HHS Public Access

Author manuscript

Oncogene. Author manuscript; available in PMC 2015 November 14.

Published in final edited form as:

Oncogene. 2015 May 14; 34(20): 2586–2596. doi:10.1038/onc.2014.195.

MutT Homolog 1 (MTH1) maintains multiple KRAS-driven pro-malignant pathways

Asmita Patel[1,2], **Dominick G. A. Burton**[1,3], **Katherine Halvorsen**[1], **Wayne Balkan**[1], **Teresita Reiner**[4], **Carlos Perez-Stable**[1,4,8], **Alexander Cohen**[1,5], **Anisleidys Munoz**[1], **Maria G. Giribaldi**[1], **Samer Singh**[6,7], **David J. Robbins**[6,8], **Dao M. Nguyen**[6,8], and **Priyamvada Rai**[1,8,9]

[1]Department of Medicine, University of Miami Miller School of Medicine, Miami, FL 33136, USA

[4]Geriatric Research, Education and Clinical Center, and Bruce W. Carter Veterans Affairs Medical Center, Miami, FL 33125, USA

[5]David and Sheila Fuente Graduate Program in Cancer Biology, University of Miami Miller School of Medicine, Miami, FL 33136, USA

[6]Department of Surgery, University of Miami Miller School of Medicine, Miami, FL 33136, USA

[8]Sylvester Comprehensive Cancer Center, University of Miami Miller School of Medicine, FL 33136, USA

Abstract

Oncogenic RAS promotes production of reactive oxygen species (ROS), which mediate pro-malignant signaling but can also trigger DNA damage-induced tumor suppression. Thus RAS-driven tumor cells require redox-protective mechanisms to mitigate the damaging aspects of ROS. Here we show that MutT Homolog 1 (MTH1), the mammalian 8-oxodGTPase that sanitizes oxidative damage in the nucleotide pool, is important for maintaining several KRAS-driven pro-malignant traits in a nonsmall cell lung carcinoma (NSCLC) model. MTH1 suppression in KRAS-mutant NSCLC cells impairs proliferation and xenograft tumor formation. Furthermore, MTH1 levels modulate KRAS-induced transformation of immortalized lung epithelial cells. MTH1 expression is upregulated by oncogenic KRAS and correlates positively with high KRAS levels in NSCLC human tumors. At a molecular level, in p53-competent KRAS-mutant cells, MTH1 loss provokes DNA damage and induction of oncogene-induced senescence (OIS). In p53-nonfunctional KRAS-mutant cells, MTH1 suppression does not produce DNA damage but induces a reduced proliferative rate and an adaptive decrease in KRAS expression levels. Thus, MTH1 not only enables evasion of oxidative DNA damage and its consequences but can also function as a molecular rheostat for maintaining oncogene expression at optimal levels. Accordingly, our results

[9]Corresponding author information: RMSB 7094, D-503, University of Miami Miller School of Medicine, 1600 NW 10th Ave, Miami, FL 33136; tel. no: (305)-243-3312; fax. no: (305)-575-3365; prai@med.miami.edu.

[2]Present address: Beckman Coulter Lifesciences, Indianapolis, IN

[3]Present address: Weizmann Institute of Science, Rehovot 76100, Israel

[7]Present address: Special Centre for Nano Sciences, Jawaharlal Nehru University, New Delhi 110067, India

Conflict of Interest

The authors declare that they have no conflict of interest.

indicate MTH1 is a novel and critical component of oncogenic KRAS-associated malignancy and its inhibition is likely to yield significant tumor-suppressive outcomes in KRAS-driven tumors.

Keywords

Nonsmall cell lung carcinoma; reactive oxygen species (ROS); DNA damage; p53; transformation; nucleotide pool

Introduction

The RAS oncogene, found in approximately 30% of all cancers, confers multiple malignant traits such as hyperproliferation, enhanced survival signaling, anoikis resistance, increased cell mobility, invasiveness, and angiogenesis [1, 2]. Many such malignant traits are mediated by oncogenic reactive oxygen species (ROS) [3, 4,5] which are elevated by chronic RAS signaling [6] through NADPH oxidase (Nox) activity and by oncogene-induced mitochondrial dysfunction [7, 8]. Thus, ROS play a dual role in RAS-transformed cells: although their elevation in oncogenic RAS-transformed cells can trigger oxidative DNA damage [7, 9] resulting in cellular senescence [9-11] or cell death [12, 13], their presence is also functionally essential to oncogenic RAS-mediated pro-malignant traits.

Hence, RAS-transformed cells must overcome ROS-associated tumor-suppressive effects without eliminating ROS production entirely, an outcome that can be accomplished by increasing levels of non-ROS-scavenging proteins that protect against oxidative damage. In this regard, the major mammalian 8-oxodGTPase, MutT Homolog 1 (MTH1) represents a unique redox-protective mechanism. MTH1 is an 18 kDa Nudix family hydrolase that selectively degrades 8-oxo-dGTP, the most pervasive oxidative DNA base modification, thus preventing its incorporation into genomic DNA during replication or repair[14]. While the long term effects of MTH1 loss are expected to be mutagenic, leading to G->T transversions, our prior work has shown that the acute effects of MTH1 suppression involve genomic strand breaks which trigger premature cell senescence[15]. We have also previously shown that MTH1 overexpression protects normal fibroblasts against HRASV12-induced cellular 8-oxoguanine accumulation, DNA damage and oncogene-induced senescence (OIS)[9], thus circumventing the first tumor suppressive step that combats oncogenic RAS-induced transformation. However, the mechanistic involvement of MTH1 in established RAS-driven tumors has not been explored. Given that MTH1 inhibits oncogene-induced DNA damage and OIS but possesses no ROS-detoxifying function, we hypothesized that MTH1 could represent an important adaptive response in activated RAS-harboring tumors due to its ability to minimize the tumor-suppressive effects of oncogenic ROS-induced oxidative DNA damage without actually eliminating ROS.

Elevated levels of MTH1 have been reported in NSCLC [16], 30-50% of which sustain KRAS mutations. However, no functional role has been ascribed to MTH1 in this aggressive tumor type nor are there studies addressing a causal association of MTH1 with KRAS status. In this study, we investigated whether modulation of MTH1 expression via stable retroviral overexpression or lentiviral shRNA-mediated suppression regulates proliferation and tumorigenicity of NSCLC cells. In addition, we determined the extent to which these effects

are driven by oncogenic KRAS or p53 status, two clinically relevant metrics that determine severity and prognosis of NSCLC. Our results support a critical role for MTH1 in facilitating oncogenic KRAS-driven transformation of lung epithelial cells, evading oxidative DNA damage-mediated induction of cellular senescence, and maintaining optimal oncogene levels in KRAS-mutant NSCLC cells that are refractory to senescence induction. Thus, our work describes the first piece of evidence implicating MTH1 as a novel facilitator of KRAS-driven malignancy in NSCLC.

Results

MTH1 suppression impairs *in vitro* and *in vivo* proliferation in KRAS-activated NSCLC cells

In order to determine whether MTH1 loss has functional consequences for the malignancy of KRAS-driven NSCLC cells, we stably knocked down MTH1 expression to > 95% using a validated lentiviral MTH1 shRNA construct [9, 15] (Fig. 1A) in the following KRAS-activated NSCLC lines: A549 (wt p53, G12S KRAS mutation), H358 (p53 null, G12C KRAS mutation) and H23 (mutant p53, G12C KRAS mutation). MTH1 suppression decreased cell proliferation in all three cell lines, with a complete proliferative arrest observed in A549 shMTH1 cells, consistent with the accompanying elevated senescence-associated beta-galactosidase (SA-beta-gal) staining (Figs. 1B, C; Supplementary Fig. S1A), increased number of persistent DNA double-strand break (DSB) gamma-H2AX/53BP1 co-localized foci relative to shGFP counterpart cells (Supplementary Fig. S1B) and a G1/S arrest (Supplementary Fig. S1C). Elevated SA-beta-gal staining and a full proliferative arrest were also observed with two other independent validated Sigma Mission® shRNA constructs targeted against MTH1 (Supplementary Figs. S1D-G). We also suppressed MTH1 in H460, another p53-competent KRAS-activated (Q61H mutation) NSCLC cell line, and found that, similar to A549, MTH1 suppression induced a senescent arrest in this cell line as well (Supplementary Fig. S2). However, the rapid proliferation rate of the H460 line selected for cells with incomplete MTH1 knockdown (Supplementary Fig. S2A, 12d point), causing these cells to overtake the bulk population in just over a week (Supplementary Fig. S2B-C). The inability of this cell line to tolerate MTH1 suppression further underscores a critical role for MTH1 in evading OIS and maintaining a high proliferation rate in KRAS-transformed cells. The p53-nonfunctional H23 or H358 cells did not undergo the proliferative arrest indicative of senescence and accordingly did not exhibit upregulated SA-beta-gal activity upon MTH1 suppression (Figs. 1B, 1C). Nor did they exhibit a G1/S arrest or differences in DSB foci formation (data not shown).

Negligible induction of shMTH1-induced cell death was observed in all the above cell lines, as ascertained by flow cytometric analysis of cell death markers, PI/Annexin V, and by cleaved PARP and cleaved caspase-3 protein expression. Minimal differences were observed in these parameters within shGFP- and shMTH1-transduced pairs for each cell line (Supplementary Figs. S3A, B). This lack of cell death upon MTH1 depletion is consistent with findings from another report in which MTH1 was downregulated via miR-145 overexpression[17].

To determine whether MTH1 knockdown also impaired proliferation in an *in vivo* setting, we monitored subcutaneous xenograft tumor formation in immunocompromised Nu/Nu

mice by shMTH1- and control shRNA-transduced counterpart cells. For the A549 cells, which rapidly undergo a senescent arrest (Fig. 1B) and therefore cannot be injected following constitutive MTH1 knockdown, we utilized a Tet-on inducible plko version [18] expressing the same hairpin sequence as the constitutive shRNA construct. The inducible version provided efficient *in vitro* and *in vivo* knockdown upon doxycycline hyclate (Dox) addition and appeared to be minimally leaky (Supplementary Fig. S4A, B). Upon Dox addition, the A549 shMTH1 cells showed significantly reduced tumor formation kinetics relative to their counterpart shLuc cells (Fig. 1D).

However, by using this inducible system, we lost the effect of MTH1 on initial tumor formation by A549 because we introduced Dox into the mice only after palpable tumors had formed. To determine whether there was any effect of MTH1 suppression on initial tumor formation efficiency in these cells, we utilized constitutive shMTH1-transduced A549 cells that had adventitiously acquired a somewhat lower (approximately 75-80%) knockdown following shRNA transduction (Fig. S4C) and thus retained slower but sustained proliferative ability relative to control cells (Supplementary Fig. S4D). Monitoring xenograft tumor formation by these cells enabled us to determine that shMTH1 induced an approximately week-long latency in A549 tumor formation at all injection sites relative to the shGFP controls and reduced the incidence as well as size of tumor formation (Supplementary Figs. S4E, F).

For the H23 and H358 lines, we used the constitutive shMTH1-transduced cells to determine the effects of MTH1 suppression on xenograft tumor formation as these cells did not fully lose proliferative capacity upon MTH1 knockdown (Fig. 1B, Supplementary Fig. S1G). In both cell lines, MTH1 suppression significantly reduced tumor formation relative to counterpart shGFP-transduced cells (Figs. 1D, E). In H23 cells, the least inherently tumorigenic of the three cell lines used (maximal tumor size being approximately 200 mm^3 compared to 500-700 mm^3 for the other two lines, 7/12 tumors per shGFP sample injection site), MTH1 suppression further reduced the size and incidence of tumor formation (4/12 sites) and delayed onset of tumor formation by approximately two weeks (Fig. 1D). Consistent with our *in vitro* data, the shMTH1-induced difference in tumor formation was not due to increased *in vivo* cell death as there was no perceptible difference in cleaved caspase-3 staining between shGFP and shMTH1 xenograft sections (Supplementary Fig. S5). Immunohistological staining of xenograft tumor sections for the Ki67 pan-proliferation marker and MTH1 expression confirmed a significant *in vivo* association between loss of MTH1 expression and reduced proliferation ability (Fig. 1F, Supplementary Fig. S6). For H23, the difference in Ki67 showed a nonsignificant ($p=0.18$) trend of decrease between the shGFP and shMTH1 tumors, likely because of the low inherent *in vivo* proliferation and tumorigenicity of this cell line (Fig. 1D). However, a visual difference in Ki67 staining between shGFP and shMTH1 tumor sections could be readily observed in several of the fields analyzed (Supplementary Fig. S6), supporting an *in vivo* shMTH1-induced defect in proliferation leading to reduced tumor formation ability. Collectively these results strongly support a functional role for MTH1 in maintaining the proliferation and tumor formation ability of oncogenic KRAS-harboring NSCLC cells.

MTH1 suppression induces distinct cell cycle inhibitors depending on p53 status

In order to ascertain the molecular basis of shMTH1-induced proliferative defects observed in the KRAS-mutant NSCLC lines, we determined whether known cell cycle inhibitors of oncogene-driven proliferation were affected. In the p53-competent A549 cells, MTH1 knockdown elevated p53 and $p21^{cip1/waf1}$ protein expression (Fig. 2A, Supplementary Fig S1E), suggesting the onset of RAS OIS [19] in agreement with the observed proliferative arrest and SA-beta-gal staining (Figs. 1B, C, Supplementary Figs. 1F,G).

In the p53-nonfunctional H23 and H358 lines which lack $p21^{cip1/waf1}$ (Fig. 2A), MTH1 suppression led to elevated levels of $p27^{kip1}$ (Fig. 2B). This molecular change was not observed in the A549 shMTH1 cells (Fig. 2B), suggesting that MTH1 loss induces different cell cycle inhibitors in the context of p53 function. This difference presumably reflects an acute (OIS) versus chronic (reduced but continued proliferation) effect of MTH1 suppression on cellular proliferative ability (Fig. 1B, A549 vs. H23, H358).

MTH1 suppression also decreased the expression of phospho-Akt (pAkt), but not phospho-Erk1/2 (pErk1/2), indicating inhibition of PI3K/Akt signaling (Fig. 2B). Activated Akt inhibition was stronger in the two p53-nonfunctional lines (~50%) when compared to A549 (~ 28%) at two weeks following MTH1 inhibition, as determined by densitometry performed on the tAkt-normalized pAkt Western blot signal between shGFP and shMTH1 counterparts. The MTH1 suppression-associated decrease in pAkt and increase in $p27^{kip1}$ was also confirmed *in vivo* in H358 shMTH1 tumor-derived lysates relative to their shGFP tumor counterparts (Fig. 2C).

To determine whether the reduction in pAkt was responsible for the observed increase in $p27^{kip1}$ [20] and ensuing proliferation defect, we stably expressed a constitutively active form of Akt, Myr-Akt, via a pBABE.neo (pBn) retroviral vector in H358 cells. We also transduced counterpart H358 cells with the empty pBn vector. We subsequently transduced each of these H358 lines with either an shGFP or shMTH1 construct. Comparing these two sets of counterpart lines showed that expression of activated Akt did not prevent $p27^{kip1}$ upregulation (Fig. 2D) nor did it rescue the shMTH1-associated reduction in proliferation (Fig. 2E). In fact, relative to the H358 pBn cells, the H358 Myr-Akt cells exhibited a greater proliferative defect under MTH1 suppression (Fig. 2E). We verified that, similar to the H358 control cells, the Myr-Akt H358 cells did not suffer from elevated cell death upon MTH1 suppression (data not shown).

MTH1 suppression-induced strand breaks require functional p53 and activated KRAS status

DNA damage can trigger tumor suppressor responses and MTH1 suppression has been reported to induce genomic DNA strand breaks[15]. In order to determine whether shMTH1 also induced DNA damage in the established KRAS-mutant NSCLC cells, we carried out the single cell gel electrophoresis or “comet” assay under alkaline conditions on shGFP or shMTH1-transduced A549, H23 and H358 cells. The alkaline assay allows assessment of DNA strand breaks as well as potential strand break-producing oxidative damage, such as persistent abasic sites. The extent of DNA damage in an individual cell is reflected in the

amount of unwound DNA migrating from the cell body under electrophoresis, and falls into one of three tail length categories: none, medium or long (Fig. 3A).

In the p53-competent A549 cells, MTH1 suppression increased the extent of alkaline DNA strand breaks i.e. the percentage of total cells with long comet tails (Fig. 3A, Supplementary Fig. S7A). However, in the p53-deficient H23 and H358 cell lines, MTH1 suppression did not increase the extent of DNA strand breakage relative to the control shGFP cells (Fig. 3A, Supplementary Fig. S7A).

To determine if this absence of shMTH1-induced DNA damage was due to the lack of functional p53, we transduced a retroviral wildtype (wt) p53 construct (pBL.p53) in the p53-null H358 cells (Fig. 3B) and then suppressed MTH1 in the wt-p53-expressing cells (Fig. 3C). Introduction of wt-p53 provoked the shMTH1 H358 cells to upregulate $p21^{cip1/waf1}$, enter senescence, and develop DNA strand breaks (Figs. 3C-E). Complementarily, suppressing p53 in the A549 cells inhibited shMTH1-induced DNA damage and cellular senescence (Supplementary Fig. S7B-F). Thus p53 appears to be functionally involved in the generation of shMTH1-induced DNA damage.

Given the increased oxidative stress produced by constitutive KRAS signaling, we wished to determine whether MTH1 suppression-induced DNA strand breaks depend on the presence of activated KRAS. For these experiments, we utilized H1563 NSCLC cells which possess functional p53 and wildtype KRAS. The H1563 cells possess significantly lower MTH1 baseline levels relative to the p53-competent KRAS-mutant A549 cells (Supplementary Fig. S8A) as well as lower total ROS levels (Supplementary Fig. S8B), suggesting a relatively reduced requirement for MTH1 in H1563 cells. We then transduced either a retroviral KRASV12-expressing construct or a control empty vector (pBp) into H1563 cells and found that in addition to elevating canonical RAS pathway proteins such as pERK and pAkt, KRASV12 also elevated MTH1 expression at both the protein and mRNA level (Fig. 3F, Supplementary Fig. S8C). As anticipated, introduction of oncogenic KRAS also increased the proliferation rate of H1563 cells (Supplementary Fig. S8D), elevated cellular ROS levels by over two-fold (Supplementary Fig. S8E) and also upregulated total 8-oxoG levels (Supplementary Fig. S8F).

Unlike their isogenic wt KRAS counterparts, the KRASV12-expressing H1563 cells showed a significant increase in SA-beta-gal activity (Fig. 3G), $p53/p21^{cip1/waf1}$ levels (Fig. 3H) and DNA strand breaks (Fig. 3I) upon MTH1 suppression. Culturing the H1563 KRASV12 cells at lower oxygen (5%) tension relative to ambient air, a condition known to reduce endogenous oxidative stress and ameliorate oncogenic RAS-associated antiproliferative effects[9, 15, 21], prior to MTH1 suppression inhibited the observed DNA strand breaks and senescent phenotype (Supplementary Figs. S8G, H). These results collectively affirm that oncogenic KRAS-harboring cells exhibit an enhanced requirement for MTH1 relative to KRAS wildtype cells, ostensibly to enable evasion of oxidative stress-induced DNA damage and OIS.

MTH1 enhances KRAS-driven oncogenic transformation in p53-abrogated lung epithelial cells

Given the relative prevalence of activating KRAS mutations in NSCLC, we wished to determine whether an *in vivo* correlation exists between MTH1 and KRAS expression levels. To do so, we used qPCR to analyze mRNA derived from a number of NSCLC and matched normal tissue samples from untreated patients for MTH1 and KRAS expression. Although the number of samples we utilized was small (n=7), we nevertheless found that sorting the samples from high-to-low KRAS levels also coordinately segregated the samples according to MTH1 levels (Fig. 4A, the black horizontal line indicating matched normal samples normalized to 1). Linear regression analysis of these data indicated there exists a positive correlation between KRAS and MTH1 levels in these human NSCLC samples (R^2=0.65) (Fig. 4A).

To determine whether MTH1 levels functionally affect KRAS-mediated oncogenic transformation, we generated stable puromycin-selectable KRASV12-expressing E6/E7 immortalized bronchial epithelial BEAS2B cells and subsequently either overexpressed or suppressed MTH1 using hygromycin-selectable vectors in the KRASV12-transformed BEAS2B cells (Fig. 4B). Empty retroviral vector (pBh) or control lentiviral shRNA (shGFP)-transduced counterpart BEAS2B cells were also established as controls. As observed in the H1563 cells (Fig. 3F), introduction of oncogenic KRAS elevated MTH1 protein levels in the BEAS2B cells (Fig. 4B; compare lanes 1 and 2). More intriguingly, MTH1 suppression led to a decrease in KRAS levels relative to shGFP counterparts (Fig. 4B compare lanes 4 vs. 5, 4C). This decrease was associated with reduced pAkt but not pErk1/2 levels, similar to what we observed in Fig. 2B (Fig. 4B). We also noticed MTH1 co-expression elevated KRAS levels relative to the cells expressing KRASV12 alone (Fig. 4B, lanes 2 vs. 3; Fig. 4C, bottom). However, given that co-introduction of the lentiviral shGFP vector also elevated KRAS levels relative to a comparable level (Fig. 4B lanes 3 vs. 4; Fig. 4C), we cannot unequivocally attribute this elevation to high MTH1 co-expression. It may be that the lentiviral transduction process selects for high KRAS-expressing cells relative to the retroviral transduction process.

Comparison of oncogenic transformation efficiency between the BEAS2B KRASV12/pBh and KRASV12/pBh.MTH1 cells via a clonogenic soft agar assay indicated that the KRASV12/MTH1 co-expressing cells produced almost twice the number of colonies than the KRASV12/pBh cells (Figs. 4D top, 4E left). Conversely MTH1 suppression in the KRASV12 cells led to a significantly reduced number of colonies relative to the control shGFP/KRASV12 cells (Figs. 4D bottom, 4E right). Thus collectively our findings indicate that MTH1 promotes oncogenic KRAS-induced transformation efficiency and maintenance of optimal oncogene levels.

Chronic MTH1 suppression reduces KRAS expression *in vitro* and *in vivo*

The major difference between the p53-competent and the p53-deficient/abrogated cells vis-à-vis MTH1 suppression appears to be an acute (senescence-associated proliferation arrest) vs. chronic (reduced but sustained proliferation) effect. Given the observed shMTH1-dependent reduction in KRAS levels in the BEAS2B cells (Fig. 4B), we speculated that a

similar phenomenon may operate in the H23 and H358 cells, particularly as these two cell lines exhibit significantly higher baseline KRAS and concomitant oncogenic ROS levels than A549 cells (Supplementary Fig. S9A, B). Accordingly we investigated whether proliferation following MTH1 suppression engendered alterations in KRAS expression in the H23 and H358 cells. Both immunoblotting (Fig. 5A, Supplementary Fig. S9C) and qPCR (Fig. 5B) indicated that KRAS levels decrease by almost 40% under chronic MTH1 suppression in both H23 and H358 cells but not in A549 cells which cease to proliferate under MTH1 suppression. This observed decrease does not occur in the H1563 KRASV12-transduced cells (Supplementary Fig. S9D), which also exhibit OIS upon MTH1 suppression (Figs. 3G-I).

The shMTH1-dependent reduction in KRAS expression is also observed *in vivo* in the H358 and H23 xenograft tumor samples (Fig. 5C, Supplementary Fig. S9E). Interestingly, the decrease in KRAS levels does not occur at an early time point (~6d post-transduction) following MTH1 suppression (Supplementary Fig. S9F) but appears to be an adaptive response over time to the loss of MTH1, again underscoring the requirement for MTH1 for maintaining optimal oncogene expression levels in KRAS-transformed NSCLC cells. Consistent with the KRAS decrease, pAkt levels in the H358 and H23 continued to decline at 18 days by 61% and 75% respectively (Fig. 5A) compared to ~ 50% at 14 days post-shMTH1-transduction (Fig. 2B). By contrast, the pAkt decline in A549 shMTH1 cells did not go beyond a 30% reduction (compared to 28% at 14 days) (Fig. 5A). Consistent with the data in Fig. 2B, pErk1/2 levels did not show a perceptible change between shGFP and shMTH1 counterparts at 18 days post-transduction either (Supplementary Fig. S9G). If the H358 shGFP and shMTH1 counterpart cells were cultured for two weeks at 5% oxygen, the lower oxygen culture inhibited the shMTH1-induced growth arrest and the decrease in KRAS and pAkt levels observed during ambient oxygen culture (Supplementary Figs. S9H, I). This finding suggested to us that the decline in KRAS levels is perhaps reflective of a cellular response to mitigate oncogene-induced intrinsic oxidative stress.

Consistent with this idea, we found that the gradual decline in KRAS was also reflected in the change in total cellular ROS levels among three KRAS-mutant NSCLC shGFP/shMTH1 pairs. In agreement with our earlier work [9, 15] and with the lack of any direct ROS detoxification functionality for MTH1, we found minimal differences in ROS levels between the shGFP and shMTH1 cells for any of three cell lines within 7 days of shRNA transduction (Fig. 5D). However, when we re-measured ROS levels approximately two weeks later, the shMTH1-transduced counterparts from both H23 and H358 cell lines exhibited a pronounced shift towards approximately 35-40% lower ROS levels whereas the A549 shMTH1 cells exhibited slightly elevated ROS levels relative to the shGFP controls (Figs. 5D, E), consistent with what has been previously been reported for senescent cells [15, 22].

It is known that Akt signaling both produces and is stimulated by ROS[23]. Given the observed shMTH1-associated progressive decline in pAkt (Fig. 2B 14d post-transduction, Fig. 5A 18d post-transduction) in H23 and H358 cells and that Myr-Akt further enhances the shMTH1-induced proliferative defect in H358 cells (Fig. 2E), we determined what happens to ROS levels in Myr-Akt H358 cells approximately 2 weeks post-transduction with

shMTH1. As expected[23], we found that introduction of Myr-Akt elevates cellular ROS levels in H358 relative to counterparts transduced with the control pBn vector (Supplementary Fig. S9J, left). However, at 18d post-transduction, whereas the H358 pBn display a reduction in cellular ROS levels relative to their shGFP counterparts, the H358 Myr-Akt cells appear unable to do so (Supplementary Fig. S9J, right).

Collectively, the above results suggest that p53-nonfunctional cells may adapt to MTH1 loss by downregulating ROS-producing mechanisms, including RAS oncogene levels and Akt signaling, and that this adaptation may allow them to continue proliferating, albeit at reduced levels. However, from our present study, we cannot exclude that other redox-regulatory and/or stress-response pathways that mediate proliferation downstream to MTH1 also contribute to this adaptive response.

Discussion

The results presented in this study strongly support the idea that oncogenic KRAS provokes an enhanced requirement for MTH1 function in NSCLC. Oncogenic KRAS elevates MTH1 levels (Figs. 3F, 4B). In turn, robust MTH1 levels are required in KRAS-activated NSCLC cells to maintain proliferation and tumorigenicity through the prevention of tumor-suppressive oxidative DNA damage or preservation of KRAS expression, oncogenic ROS levels and Akt signaling (summarized in Fig. 5F). Accordingly, the overall effect of suppressing MTH1 in KRAS-driven NSCLC cells is either induction of a senescent arrest or selection of slower-proliferating subpopulations with reduced pro-malignant molecular traits.

Our study indicates two different mechanisms operate to inhibit KRAS-induced malignancy in NSCLC cells when MTH1 expression is suppressed. In a p53-competent context, MTH1 suppression induces an acute effect via OIS-induced cessation of proliferation, resulting from oncogenic KRAS-induced genomic DNA strand breaks (Figs. 1B,C; Fig. 3). Although our study suggests induction of DNA damage in response to MTH1 suppression depends stringently on functional p53 (Fig. 3, Supplementary Fig. S7), the exact molecular mechanism(s) by which MTH1 suppression induces DNA damage is as yet unelucidated. It is known NSCLC cells sustain lost or impaired 8-oxoguanine glycosylase (hOGG1) activity [24, 25], and it has further been suggested that this deficiency leaves MTH1 as the predominant inhibitor of genomic 8-oxoG accumulation in NSCLC cells [26]. Thus we speculate that reduced MTH1 expression and function in the context of impaired hOGG1 activity and RAS oncogene-induced genotoxic stress is likely to disrupt base excision repair coordination and efficient ligation at multiple genomic 8-oxoG sites [27], leading to unrepaired DNA damage. An analogous mechanism has been recently identified involving uracil-N-glycosylase (UNG) activity-induced DNA damage in tumor cells in the presence of elevated genomic dUTP incorporation [28].

The second tumor suppressor mechanism invoked by MTH1 suppression occurs in a p53-nonfunctional context and provides insights into the chronic effects of MTH1 loss, whereby the MTH1-suppressed cells do not entirely lose proliferative ability. As p53 is lost or mutated in 50% of tumors, this effect of MTH1 suppression is likely to be translationally

important. MTH1 inhibition in p53-nonfunctional H23 and H358 cell lines does not produce DNA damage relative to control cells (Fig. 3A), which is consistent with the ability of these cells to survive and proliferate despite MTH1 suppression. It is likely that the p53-deficient status of H358 and H23 cells has caused them to acquire compensatory mechanisms that enable proliferation despite pervasive genomic instability. The inability of MTH1 suppression to elevate DNA strand breakage in these cells likely reflects the consequences of such compensation. Additionally p53 can modulate cellular ROS levels through a number of pro-oxidant mechanisms[29] and control base excision repair mechanisms that remove genomic 8-oxoG[30], both factors which could contribute to p53-nonfunctional cells not incurring shMTH1-induced DNA damage. Thus while a definitive molecular delineation of p53's role in this phenomenon is likely to be complicated and beyond the scope of this study, our findings are consistent with the idea that nonfunctional p53 confers resistance to DNA damaging agents [31, 32].

Nevertheless, we find MTH1 suppression in the p53-nonfunctional H358 and H23 cells reduced *in vitro* and *in vivo* proliferation and elevated $p27^{kip1}$ expression, both positive prognostic factors for KRAS-driven NSCLC[33]. More significantly, MTH1 suppression in the p53-nonfunctional cells reduced KRAS expression *in vitro* and *in vivo* (Fig. 5). Several studies have shown that reducing levels of oncogenic KRAS impairs proliferative and tumorigenic capacity in NSCLC and other RAS-driven tumor cells [34-37]. Thus, MTH1 inhibition ostensibly suppresses the propagation of high KRAS-expressing cells, which possess concomitantly greater capacity for malignant growth and signaling. Furthermore, the shMTH1-associated reduction in pAkt levels (Figs. 2B, 2C, 5A) is very similar to what was observed in KRAS-suppressed H23 and H358 cells lines in another study [35]. Previous studies have established a critical role for ROS in promoting hyperactivated Akt signaling and RAS-driven tumorigenesis [38, 39]. Thus the observed reduction in ROS levels in shMTH1 H23 and H358 cells (Figs. 5D, E) likely also impacts the observed decrease in activated Akt (Figs. 2B, 2C, Fig. 5A). Furthermore, inhibition of Akt signaling is associated with resistance to RAS-induced oxidative stress and antiproliferative effects[23]. This is consistent with our findings regarding the shMTH1-induced reduction in Akt signaling in proliferating H23 and H358 cells (Figs. 2B, 5A) as well as the enhancement of shMTH1-induced proliferation defect in H358 Myr-Akt cells (Fig. 2E) which do not exhibit a decrease in cellular ROS levels upon MTH1 suppression (Supplementary Fig. S9J).

Further studies will be required to understand the mechanisms by which MTH1 can act as a molecular rheostat for KRAS levels and accordingly its downstream pro-malignant effects. The KRAS promoter consists of G-rich tracts[40], which constitute hotspots for 8-oxoG accumulation and concomitant DNA breaks[41] either via direct oxidation or incorporation of 8-oxo-dGTP. Thus continued proliferation and DNA replication under MTH1 suppression could either lead to KRAS promoter mutation through elevated 8-oxoG[41] or 8-oxoG-associated structural alterations in promoter G-quadruplexes[40, 42, 43]. Such a possibility would also explain the gradual rather than acute nature of KRAS decrease as it would take several replication cycles to produce steady-state oxidative damage in the KRAS promoter region.

It has proven difficult to directly target oncogenic RAS in tumors [44]. The ability of MTH1 suppression to provoke DNA damage-induced OIS or downregulate oncogene levels and concurrent downstream traits such as transformation and proliferation suggests that targeting MTH1 in lieu of KRAS is likely to produce similar tumor-inhibitory effects. Two recent articles[45, 46] published while our manuscript was in revision characterize synthetic MTH1 inhibitors and support our conclusions that pharmacologic inhibition of MTH1 in human tumors possesses significant therapeutic promise. Thus we believe the findings presented herein provide valuable context for targeting MTH1 in KRAS-driven NSCLC and potentially other KRAS-driven tumors.

Materials and Methods

Human tissue-derived experiments

All human subjects research was carried out according to protocols and consent guidelines approved by the University of Miami Institutional Review Board (IRB). Retrospective frozen tissue samples consisting of de-identified matched normal and tumor pairs were obtained from untreated patients diagnosed with Stage 1, 2 or 3 NSCLC at Sylvester Comprehensive Cancer Center, Miami, FL.

Cell lines and culture

BEAS2B, A549, H460, H23, H358 and H1563 cells were obtained from the American Type Culture Collection (ATCC). All cells were grown at 37°C in 21% oxygen or 5% oxygen where indicated and 5% CO_2. BEAS2B cells were maintained in DMEM:F12 complete base media supplemented with 10% fetal bovine serum (FBS) and 100 units/ml penicillin/streptomycin. A549, H23, H358 and H1563 cells were maintained in RPMI-1640 complete base media supplemented with 10% FBS and 100 units/ml penicillin/streptomycin (Gibco, Life Technologies).

Soft agar colony formation assay

Noble agar (DIFCO) at a 2.4% stock concentration was added to a solution containing DMEM, 20% FBS and 200 units of streptomycin:penicillin/fungizone to yield a 0.6% bottom agar solution. A 0.3% top agar solution containing suspended target cells was layered over pre-solidified bottom agar in 6 cm dishes. The assay was set up in triplicate per sample, with 10^4 cells seeded per dish. Once a week, the top agar was refreshed with 100-200 μl fresh complete media. Three weeks post-seeding, the dishes were imaged and the colonies scored using the Quantity One software on a Chemidoc (BioRad) machine.

DNA constructs and viral transduction

The pBABE.MTH1 overexpression and pBLIC (pBL).p53 retroviral constructs were cloned in our laboratory[9, 47]. The retroviral pBABE.puro.KRASV12 construct (Addgene plasmid 9052), the pBABE.neo.Myr-AKT1 (15266) and the inducible lentiviral plko-TET-on backbone [18] construct were obtained from Addgene. Viral supernatant production in HEK 293T cells and infection of target cells were performed as described previously [48]. Transduced cells were selected in 2.5 μg/ml puromycin-containing, 100 μg/ml hygromycin-containing, 10 μg/ml blastocidin-containing or 500 μg/ml G418-containing media for a

minimum period of 5-7 days (corresponding to the time taken for untransduced cells to die completely in selection media).

The plko.shMTH1 and plko.shGFP constructs have been previously described [9, 15]. The plko-Tet-on.shMTH1 target sequence is the same as the constitutive shMTH1 target. The plko-Tet-on.shLuc target sequence is: 5′ CTTCGAAATGTCCGTTCGGTT 3′. Two additional Sigma Mission shMTH1 constructs used in the Supplementary data section were targeted to the following sequences:

shMTH1-2 (TRCN0000288947): 5’ CCTGAGCTCATGGACGTGCAT 3’

shMTH1-3 (TRCN0000050132): 5’ CGAGTTCTCCTGGGCATGAAA 3’

Cell Proliferation Measurements

To determine cell proliferation rates, 5×10^4 were seeded in 10 cm dishes and cell counts were carried out in triplicate every 24 hours over a four-day period, via a hemocytometer. Fresh media was added every 2-3 days to dishes not being counted. A minimum of two independent cell proliferation curves was established per sample pair being assayed.

Western blotting

Western blotting was carried out as previously described [47]. Blots were probed with antibodies against the following proteins: MTH1 (NB100-109, Novus Biologicals), p53 (sc-126, Santa Cruz Biotech), $p21^{cip1/waf1}$ (sc-817, Santa Cruz Biotech), phospho-Akt (4060, Cell Signaling) total Akt (9272, Cell Signaling), cleaved-PARP (9541, Cell Signaling), p-Erk1/2 (9101, Cell Signaling), total Erk (9102, Cell Signaling), $p27^{kip1}$ (sc-528, Santa Cruz Biotech), KRAS (sc-30, Santa Cruz Biotech), tubulin (sc-8035, Santa Cruz Biotech), actin (ab82266, Abcam) and GAPDH (ab9485, Abcam). Western blotting images represent data consistent with a minimum of two independently established sets of samples. Densitometry of images was carried out via the ImageJ Analyze Gels module.

Quantitative PCR (qPCR) analysis

The mRNA preparation from the tumor samples was accomplished as described previously [49] using the Trizol method and the mRNA Easy kit. Using 1.0μg of RNA, cDNA was synthesized with the High Capacity cDNA Reverse Transcription kit (Applied Biosystems, cat# 4368814). The qPCR reaction was set up with 1.0μl of cDNA and 20X TaqMan probes and TaqMan Universal PCR Master Mix (Applied Biosystems cat# 4324018) in a 15μl total volume. Samples were run in triplicate on an Applied Biosystem Real-Time machine using a StepOne program consisting of 95°C for 10 minutes and 40 cycles of the following: 95°C for 15 seconds and 60°C for 1 minute. Gene expression levels were calculated using the $2^{-\Delta\Delta C_T}$ method[50]. The following gene-specific TaqMan primer/probe sets were used: MTH1 (Hs00159343_m1), KRAS (Hs00364282_m1), ActinB (internal normalization control; Hs99999903_m1)

ROS measurements

The assay was carried out as described previously [15, 51] via staining with 10 μM 5- (and-6)-chloromethyl-2′,7′-dichlorofluorescein diacetate (CM-DCF-DA; Molecular Probes/Life

Technologies, C6827) for 25 min at 37°C. Flow cytometric analysis was conducted on an Accuri C6 cytometer (BD Biosciences).

Comet assay

The comet assay was carried out according to the Trevigen Comet Assay kit instructions for alkaline unwinding and electrophoresis conditions. Gel electrophoresis was carried out at 21V for 30 min at 4 °C. Positive and negative control cells provided by Trevigen were run along with each sample to ensure that any lack of “tails” in a sample or long “tails” were not due to technical issues. A minimum of 100 individual cells per sample were scored in duplicate from two independent experiments, with the DNA tail lengths being visually categorized as either long, medium or none in double-blind scoring.

Senescence Associated Beta-gal assay

SA-beta-gal staining was carried out as described elsewhere [51, 52]. To quantify positive staining, >100 cells were counted for each sample over multiple fields of view, excluding fields at the very edge. Results represent data from a minimum of two independent experiments.

Xenograft tumor experiments

All animal protocols were approved by the University of Miami Institutional Animal Care and Use Committee (IACUC). Approximately 10^6 cells were resuspended in 100 μL of Matrigel (BD Biosciences), diluted 1:2 in RPMI-1640 media and injected subcutaneously using a 25-gauge needle into the flanks of six-week old immunocompromised mice (Nu/Nu; Harlan Laboratories, Inc.). A minimum of 12 sites was injected per sample. Tumor length, width and height were measured biweekly using electronic precision calipers (VWR). Tumor volumes were calculated according to the following formula: 4/3*3.14*(height/2*width/2*length/2) or 0.52*(height*width*length). Tumor–bearing animals were euthanized before tumors could exceed a volume of 1 cm^3.

For the animals injected with plko-Tet-on inducible shRNA constructs, once palpable tumors were observed (around 14 days post-injection), both the shLuc and shMTH1 groups were continuously dosed via oral ingestion with 2mg/ml doxycycline hyclate (Sigma) in a 5% sucrose solution.

Immunohistological and double immunofluorescent (DIF) staining

For immunostaining, tissues were fixed overnight in formalin and stained for human MTH1 (1/150 dilution; Novus Biologicals) and pan-proliferation marker Ki67 (1/500 dilution; NCL-Ki67p, Leica Microsystems) as described previously[53]. Images were photographed using a Nikon Microphot-FXA microscope and a Nikon Coolpix 4300 digital camera. For quantification, three random high-powered (200X) fields (hpf) from each section were counted for a minimum of five different tumors per sample (four for H23 shMTH1 to include all tumors formed at sites of injection). Double immunofluorescent staining (DIF) was carried out using the MTH1 (1/150 dilution) and KRAS (1/100 dilution) antibodies, followed by incubation with AlexaFluor 488 and 594 IgG secondary antibodies (1/500 dilution; Invitrogen) and DAPI mounting medium (Vector Laboratories). Images were

captured using a Nikon Eclipse 90i fluorescence microscope and merged using Adobe Photoshop.

Statistical analysis

Results are presented as mean ± standard deviation. Data were analyzed by unpaired two-tailed Student's t-test and results with p-values <0.05 considered statistically significant.

Supplementary Material

Refer to Web version on PubMed Central for supplementary material.

Acknowledgements

We thank Dr. Ramiro Verdun for helpful discussions, and Karen Alvarez Delfin for technical assistance. This work was supported by a James and Esther King Florida Biomedical New Investigator Research grant, a University of Miami Dean's Bridge Fund award and an NIH/NCI grant (R01CA175086) to P.R.

References

1. Campbell PM, Der CJ. Oncogenic Ras and its role in tumor cell invasion and metastasis. Semin Cancer Biol. 2004; 14:105–114. [PubMed: 15018894]
2. Rajalingam K, Schreck R, Rapp UR, Albert S. Ras oncogenes and their downstream targets. Biochim Biophys Acta. 2007; 1773:1177–1195. [PubMed: 17428555]
3. Mitsushita J, Lambeth JD, Kamata T. The superoxide-generating oxidase Nox1 is functionally required for Ras oncogene transformation. Cancer Res. 2004; 64:3580–3585. [PubMed: 15150115]
4. Arbiser JL, Petros J, Klafter R, Govindajaran B, McLaughlin ER, Brown LF, et al. Reactive oxygen generated by Nox1 triggers the angiogenic switch. Proc Natl Acad Sci U S A. 2002; 99:715–720. [PubMed: 11805326]
5. Weinberg F, Hamanaka R, Wheaton WW, Weinberg S, Joseph J, Lopez M, et al. Mitochondrial metabolism and ROS generation are essential for Kras-mediated tumorigenicity. Proc Natl Acad Sci U S A. 2010; 107:8788–8793. [PubMed: 20421486]
6. Irani K, Xia Y, Zweier JL, Sollott SJ, Der CJ, Fearon ER, et al. Mitogenic Signaling Mediated by Oxidants in Ras-Transformed Fibroblasts. Science. 1997; 275:1649–1652. [PubMed: 9054359]
7. Moiseeva O, Bourdeau V, Roux A, Deschenes-Simard X, Ferbeyre G. Mitochondrial dysfunction contributes to oncogene-induced senescence. Mol Cell Biol. 2009; 29:4495–4507. [PubMed: 19528227]
8. Finkel T. Intracellular redox regulation by the family of small GTPases. Antioxid Redox Signal. 2006; 8:1857–1863. [PubMed: 16987038]
9. Rai P, Young JJ, Burton DG, Giribaldi MG, Onder TT, Weinberg RA. Enhanced elimination of oxidized guanine nucleotides inhibits oncogenic RAS-induced DNA damage and premature senescence. Oncogene. 2011; 30:1489–1496. [PubMed: 21076467]
10. Mallette FA, Gaumont-Leclerc M-F, Ferbeyre G. The DNA damage signaling pathway is a critical mediator of oncogene-induced senescence. Genes Dev. 2007; 21:43–48. [PubMed: 17210786]
11. Di Micco R, Fumagalli M, Cicalese A, Piccinin S, Gasparini P, Luise C, et al. Oncogene-induced senescence is a DNA damage response triggered by DNA hyper-replication. Nature. 2006; 444:638–642. [PubMed: 17136094]
12. Liou JS, Chen CY, Chen JS, Faller DV. Oncogenic ras mediates apoptosis in response to protein kinase C inhibition through the generation of reactive oxygen species. J Biol Chem. 2000; 275:39001–39011. [PubMed: 10967125]
13. Chen CY, Liou J, Forman LW, Faller DV. Correlation of genetic instability and apoptosis in the presence of oncogenic Ki-Ras. Cell Death Differ. 1998; 5:984–995. [PubMed: 9846185]

14. Nakabeppu Y. Molecular genetics and structural biology of human MutT homolog, MTH1. Mutation Research-Fundamental and Molecular Mechanisms of Mutagenesis. 2001; 477:59–70. [PubMed: 11376687]
15. Rai P, Onder TT, Young JJ, McFaline JL, Pang B, Dedon PC, et al. Continuous elimination of oxidized nucleotides is necessary to prevent rapid onset of cellular senescence. Proc Natl Acad Sci U S A. 2009; 106:169–174. [PubMed: 19118192]
16. Kennedy CH, Pass HI, Mitchell JB. Expression of human MutT homologue (hMTH1) protein in primary non-small-cell lung carcinomas and histologically normal surrounding tissue. Free Radical Biology and Medicine. 2003; 34:1447–1457. [PubMed: 12757855]
17. Cho WC, Chow AS, Au JS. MiR-145 inhibits cell proliferation of human lung adenocarcinoma by targeting EGFR and NUDT1. RNA biology. 2011; 8:125–131. [PubMed: 21289483]
18. Wiederschain D, Wee S, Chen L, Loo A, Yang G, Huang A, et al. Single-vector inducible lentiviral RNAi system for oncology target validation. Cell Cycle. 2009; 8:498–504. [PubMed: 19177017]
19. Serrano M, Lin AW, McCurrach ME, Beach D, Lowe SW. Oncogenic ras Provokes Premature Cell Senescence Associated with Accumulation of p53 and p16INK4a. Cell. 1997; 88:593–602. [PubMed: 9054499]
20. Collado M, Medema RH, Garcia-Cao I, Dubuisson ML, Barradas M, Glassford J, et al. Inhibition of the phosphoinositide 3-kinase pathway induces a senescence-like arrest mediated by p27Kip1. J Biol Chem. 2000; 275:21960–21968. [PubMed: 10791951]
21. Lee AC, Fenster BE, Ito H, Takeda K, Bae NS, Hirai T, et al. Ras Proteins Induce Senescence by Altering the Intracellular Levels of Reactive Oxygen Species. J Biol Chem. 1999; 274:7936–7940. [PubMed: 10075689]
22. Takahashi A, Ohtani N, Yamakoshi K, Iida S-i, Tahara H, Nakayama K, et al. Mitogenic signalling and the p16INK4a-Rb pathway cooperate to enforce irreversible cellular senescence. Nat Cell Biol. 2006; 8:1291–1297. [PubMed: 17028578]
23. Nogueira V, Park Y, Chen CC, Xu PZ, Chen ML, Tonic I, et al. Akt determines replicative senescence and oxidative or oncogenic premature senescence and sensitizes cells to oxidative apoptosis. Cancer Cell. 2008; 14:458–470. [PubMed: 19061837]
24. Janik J, Swoboda M, Janowska B, Ciesla JM, Gackowski D, Kowalewski J, et al. 8-Oxoguanine incision activity is impaired in lung tissues of NSCLC patients with the polymorphism of OGG1 and XRCC1 genes. Mutat Res. 2011; 709-710:21–31. [PubMed: 21376741]
25. Wikman H, Risch A, Klimek F, Schmezer P, Spiegelhalder B, Dienemann H, et al. hOGG1 polymorphism and loss of heterozygosity (LOH): significance for lung cancer susceptibility in a caucasian population. Int J Cancer. 2000; 88:932–937. [PubMed: 11093817]
26. Speina E, Arczewska KD, Gackowski D, Zielinska M, Siomek A, Kowalewski J, et al. Contribution of hMTH1 to the Maintenance of 8-Oxoguanine Levels in Lung DNA of Non-Small-Cell Lung Cancer Patients. J Natl Cancer Inst. 2005; 97:384–395. [PubMed: 15741575]
27. Dobbs TA, Palmer P, Maniou Z, Lomax ME, O'Neill P. Interplay of two major repair pathways in the processing of complex double-strand DNA breaks. DNA Repair (Amst). 2008; 7:1372–1383. [PubMed: 18571480]
28. Hu CM, Yeh MT, Tsao N, Chen CW, Gao QZ, Chang CY, et al. Tumor cells require thymidylate kinase to prevent dUTP incorporation during DNA repair. Cancer Cell. 2012; 22:36–50. [PubMed: 22789537]
29. Liu B, Chen Y, St Clair DK. ROS and p53: a versatile partnership. Free Radic Biol Med. 2008; 44:1529–1535. [PubMed: 18275858]
30. Zhou J, Ahn J, Wilson SH, Prives C. A role for p53 in base excision repair. EMBO J. 2001; 20:914–923. [PubMed: 11179235]
31. Fan S, el-Deiry WS, Bae I, Freeman J, Jondle D, Bhatia K, et al. p53 gene mutations are associated with decreased sensitivity of human lymphoma cells to DNA damaging agents. Cancer Res. 1994; 54:5824–5830. [PubMed: 7954409]
32. Lee JM, Bernstein A. p53 mutations increase resistance to ionizing radiation. Proc Natl Acad Sci U S A. 1993; 90:5742–5746. [PubMed: 8516323]

33. Hommura F, Dosaka-Akita H, Mishina T, Nishi M, Kojima T, Hiroumi H, et al. Prognostic significance of p27KIP1 protein and ki-67 growth fraction in non-small cell lung cancers. Clin Cancer Res. 2000; 6:4073–4081. [PubMed: 11051259]
34. Brummelkamp TR, Bernards R, Agami R. Stable suppression of tumorigenicity by virus-mediated RNA interference. Cancer Cell. 2002; 2:243–247. [PubMed: 12242156]
35. Sunaga N, Shames DS, Girard L, Peyton M, Larsen JE, Imai H, et al. Knockdown of oncogenic KRAS in non-small cell lung cancers suppresses tumor growth and sensitizes tumor cells to targeted therapy. Mol Cancer Ther. 2011; 10:336–346. [PubMed: 21306997]
36. Shirasawa S, Furuse M, Yokoyama N, Sasazuki T. Altered growth of human colon cancer cell lines disrupted at activated Ki-ras. Science. 1993; 260:85–88. [PubMed: 8465203]
37. Mukhopadhyay T, Tainsky M, Cavender AC, Roth JA. Specific inhibition of K-ras expression and tumorigenicity of lung cancer cells by antisense RNA. Cancer Res. 1991; 51:1744–1748. [PubMed: 1998965]
38. Cao J, Schulte J, Knight A, Leslie NR, Zagozdzon A, Bronson R, et al. Prdx1 inhibits tumorigenesis via regulating PTEN/AKT activity. EMBO J. 2009; 28:1505–1517. [PubMed: 19369943]
39. Nogueira V, Hay N. Molecular Pathways: Reactive Oxygen Species Homeostasis in Cancer Cells and Implications for Cancer Therapy. Clin Cancer Res. 2013
40. Cogoi S, Xodo LE. G-quadruplex formation within the promoter of the KRAS protooncogene and its effect on transcription. Nucleic Acids Res. 2006; 34:2536–2549. [PubMed: 16687659]
41. Clark DW, Phang T, Edwards MG, Geraci MW, Gillespie MN. Promoter G-quadruplex sequences are targets for base oxidation and strand cleavage during hypoxia-induced transcription. Free Radic Biol Med. 2012; 53:51–59. [PubMed: 22583700]
42. Szalai VA, Singer MJ, Thorp HH. Site-specific probing of oxidative reactivity and telomerase function using 7,8-dihydro-8-oxoguanine in telomeric DNA. Journal of the American Chemical Society. 2002; 124:1625–1631. [PubMed: 11853436]
43. Ghosh A, Rossi ML, Aulds J, Croteau D, Bohr VA. Telomeric D-loops containing 8-oxo-2′-deoxyguanosine are preferred substrates for Werner and Bloom syndrome helicases and are bound by POT1. J Biol Chem. 2009; 284:31074–31084. [PubMed: 19734539]
44. Downward J. Targeting RAS signalling pathways in cancer therapy. Nature reviews Cancer. 2003; 3:11–22. [PubMed: 12509763]
45. Huber KV, Salah E, Radic B, Gridling M, Elkins JM, Stukalov A, et al. Stereospecific targeting of MTH1 by (S)-crizotinib as an anticancer strategy. Nature. 2014; 508:222–227. [PubMed: 24695225]
46. Gad H, Koolmeister T, Jemth AS, Eshtad S, Jacques SA, Strom CE, et al. MTH1 inhibition eradicates cancer by preventing sanitation of the dNTP pool. Nature. 2014; 508:215–221. [PubMed: 24695224]
47. Patel A, Munoz A, Halvorsen K, Rai P. Creation and validation of a ligation-independent cloning (LIC) retroviral vector for stable gene transduction in mammalian cells. BMC biotechnology. 2012; 12:3. [PubMed: 22248071]
48. Stewart SA, Dykxhoorn DM, Palliser D, Mizuno H, Yu EY, An DS, et al. Lentivirus-delivered stable gene silencing by RNAi in primary cells. RNA. 2003; 9:493–501. [PubMed: 12649500]
49. Fei DL, Li H, Kozul CD, Black KE, Singh S, Gosse JA, et al. Activation of Hedgehog signaling by the environmental toxicant arsenic may contribute to the etiology of arsenic-induced tumors. Cancer Res. 2010; 70:1981–1988. [PubMed: 20179202]
50. Schmittgen TD, Livak KJ. Analyzing real-time PCR data by the comparative C(T) method. Nature protocols. 2008; 3:1101–1108. [PubMed: 18546601]
51. Burton DG, Giribaldi MG, Munoz A, Halvorsen K, Patel A, Jorda M, et al. Androgen deprivation-induced senescence promotes outgrowth of androgen-refractory prostate cancer cells. PloS one. 2013; 8:e68003. [PubMed: 23840802]
52. Dimri G, Lee X, Basile G, Acosta M, Scott G, Roskelley C, et al. A Biomarker that Identifies Senescent Human Cells in Culture and in Aging Skin in vivo. PNAS. 1995; 92:9363–9367. [PubMed: 7568133]

53. Reiner T, de las Pozas A, Perez-Stable C. Sequential combinations of flavopiridol and docetaxel inhibit prostate tumors, induce apoptosis, and decrease angiogenesis in the Ggamma/T-15 transgenic mouse model of prostate cancer. Prostate. 2006; 66:1487–1497. [PubMed: 16921509]

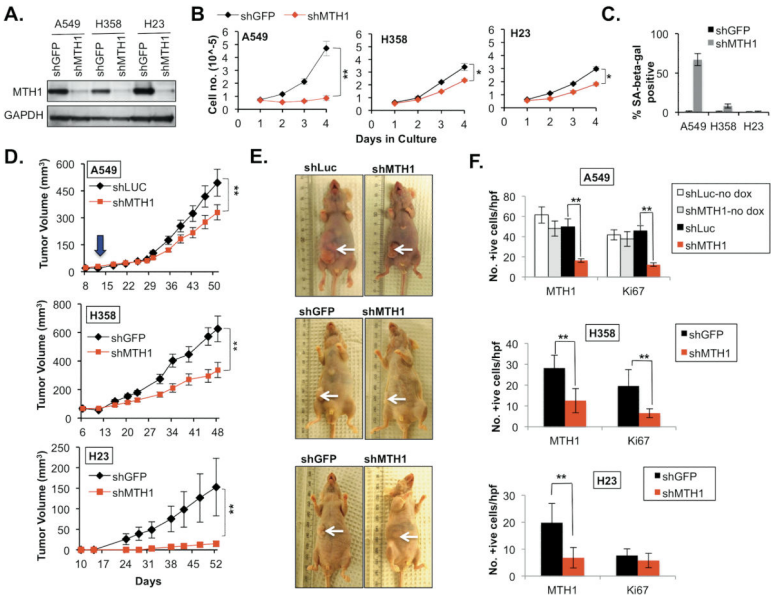

Figure 1. MTH1 suppression induces an in vitro and in vivo proliferation defect in KRAS-mutant NSCLC cells

(A) MTH1 suppression via lentiviral shRNA. Immunoblotting for MTH1 expression was carried out against approximately 25 μg of protein lysates derived from the indicated NSCLC cell lines transduced with either plko.shGFP or plko.shMTH1 to confirm MTH1 knockdown. GAPDH was used to normalize for protein loading.

(B) Proliferation rates in the indicated samples transduced with either shGFP or shMTH1. **p<0.01, *p<0.05.

(C) SA-beta-gal activity. As described in the Methods section, SA-beta-gal staining was assayed and quantitated in the indicated samples.

(D) MTH1 suppression reduces xenograft tumor formation by KRAS-mutant NSCLC cells. Tumor formation kinetics are shown for the indicated samples. For A549 cells, which were transduced with either the Tet-on shLuc or shMTH1 constructs, doxycycline was administered to the animals at day 14 post-injection (indicated by an arrow on the tumor growth curves).

(E) Representative images of animals used in the xenograft studies. Animals from each group are shown to the right of the respective tumor curves in (D). White arrows indicate sites of subcutaneous tumors. Tumor incidences (tumors formed/sites injected) were as follows: A549 shLuc and shMTH1: 12/12; H358 shGFP: 13/13, H358 shMTH1: 12/13; H23 shGFP: 7/12, H23 shMTH1: 4/12. **p < 0.01.

(F) In vivo correlation between MTH1 and proliferation. Quantification of immunohistochemical staining for Ki67 and MTH1 is shown for the indicated samples as number of positively stained cells/high-powered field (hpf) counted.

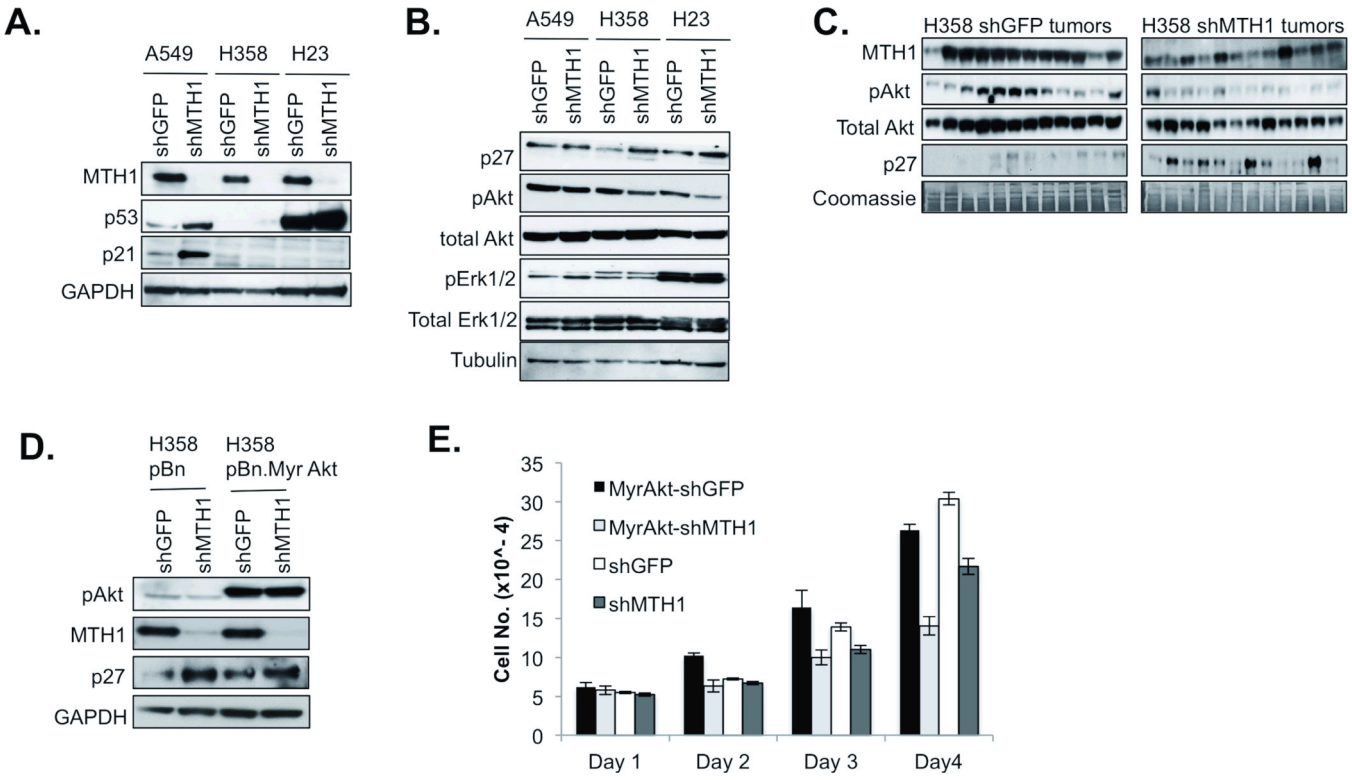

Figure 2. Molecular effects of MTH1 suppression in KRAS-mutant NSCLC cells

(A)-(C) Immunoblotting using 20 μg protein lysates was carried out against the indicated proteins. Cell pellets were harvested approximately 14 days post-transduction (the A549 cells were harvested 8 days post-transduction).

(A) MTH1 suppression elevates p53/p21$^{cip1/waf1}$ in p53-competent NSCLC cells. GAPDH is used as a loading normalization control.

(B) MTH1 suppression elevates p27^{kip1} and reduces pAkt in p53-noncompetent H358 and H23 NSCLC cells. Tubulin is used as a normalization control.

(C) *In vivo* shMTH1 effects in H358 xenograft tumors recapitulate *in vitro* effects. Immunoblotting using 20 μg protein lysate from H358 xenograft tumor samples was carried out using the indicated antibodies. Coomassie blue total protein staining was used as a loading control.

(D) H358 cells were transduced with either pBneo (pBn) or pBn. Myr-Akt and then selected in G418-containing media. Following successful selection, each counterpart was transduced with either shGFP or shMTH1. Cells were harvested and total protein lysates produced approximately 16 days following shRNA transduction. Immunoblotting was carried out on 20 μg of total protein against the indicated antibodies.

(E) Relative cell proliferation rates. The four cell lines from (D) were each seeded at 5×10^4 on Day 0 and the number of cells counted (in triplicate) for the next four days.

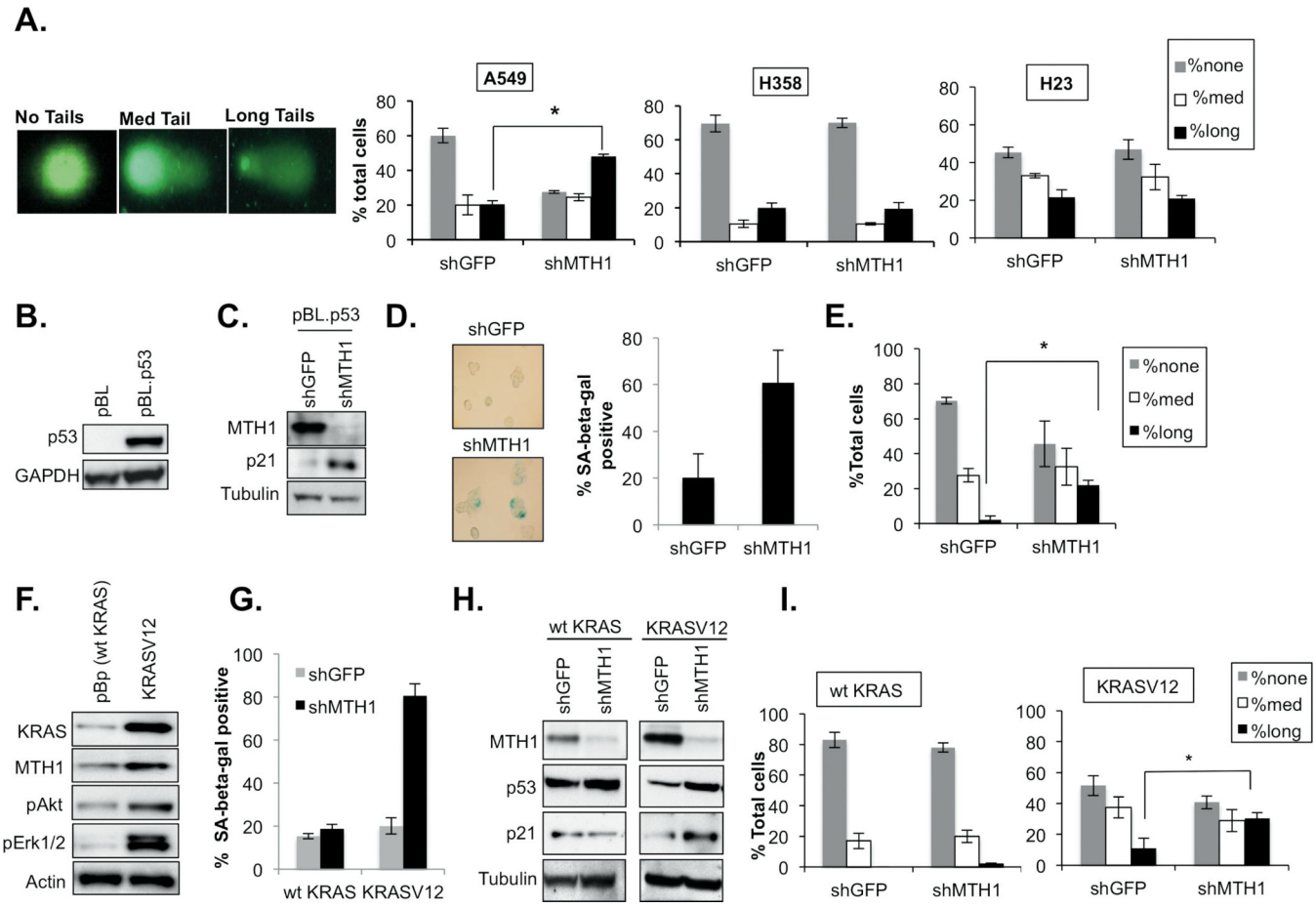

Figure 3. MTH1 suppression-induced DNA damage is provoked by the presence of functional p53 and activating KRAS mutations

(A) p53 is required for shMTH1-induced DNA strand breaks. Alkaline comet assay data is shown the indicated samples. Representative single cell images used for scoring within the three categories are shown next to the quantitation. *p<0.05.

(B) Wildtype p53 overexpression in p53-null H358 cells. Immunoblotting for p53 is shown in H358 cells transduced with either the empty pBL vector or the pBL vector expressing wildtype p53.

(C) MTH1 suppression in pBL.p53 H358 cells. Immunoblotting was carried out against the indicated proteins using 15 μg protein lysates.

(D) SA-beta-gal staining in pBL.p53 H358 cells with either shGFP or shMTH1. Representative images and quantitation of staining are shown.

(E) Quantitation of alkaline comet assay results for shGFP and shMTH1-transduced H358-p53 cells, *p <0.05.

(F) Oncogenic KRAS elevates MTH1 expression. Immunoblotting was carried out against the indicated proteins in pBABE.KRASV12- or pBABE.puro backbone-transduced (pBp, wt KRAS) H1563 cells.

(G) Comparison of shMTH1 effects on SA-beta-gal staining in the control and KRASV12 transduced H1563.

(H) Oncogenic KRAS is required for upregulated p53/$p21^{cip1/waf1}$. Approximately 15 μg of protein lysates were probed with the indicated antibodies.
(I) Comparison of shMTH1 effects on DNA strand breaks in the wt and KRASV12 H1563. The alkaline comet assay was carried out on the indicated samples and the different forms of damage quantitated and graphed, *$p<0.05$.

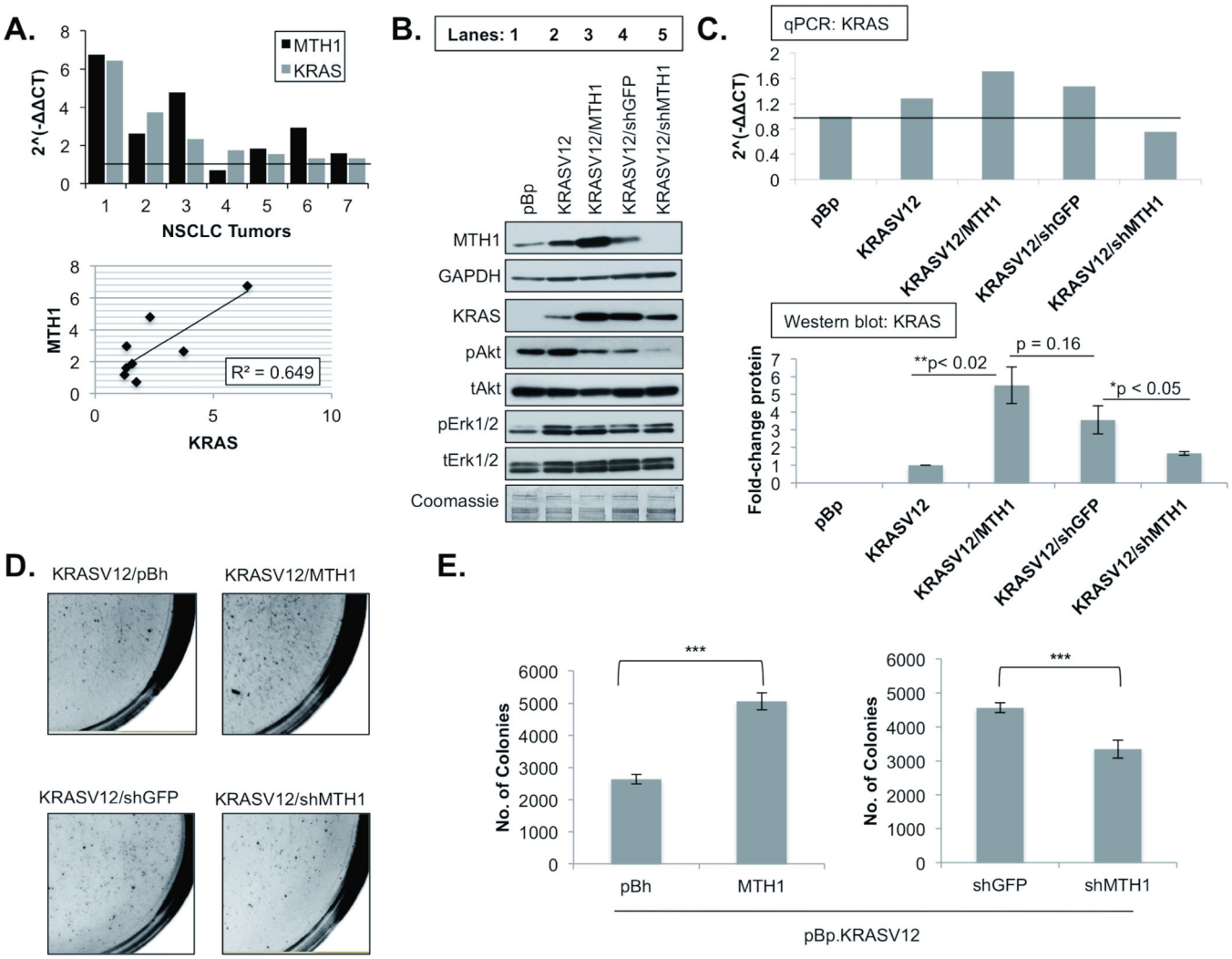

Figure 4. MTH1 promotes maintenance of oncogenic KRAS levels and modulates transformation efficiency

(A) High KRAS levels in human NSCLC tumors correlate with high MTH1 levels. A qPCR analysis of MTH1 and KRAS mRNA levels in matched tumor/adjacent normal NSCLC samples from untreated patients is shown. ActinB was used for normalization. All matched normal tissue values were set at 1 (indicated by a black horizontal line). Linear regression analysis is shown below the qPCR analysis and was carried out using Microsoft Excel macro.

(B) MTH1 levels promote maintenance of KRAS expression. BEAS2B cells were transformed with KRASV12 as described in the Results section and then transduced with either an MTH1 overexpression construct, shMTH1 construct or counterpart control vectors. Immunoblotting was carried out on 15 μg of lysates from the indicated samples, expressing either a control vector (pBp), KRASV12, KRASV12 in conjunction with pBh.MTH1 (KRASV12/MTH1) or KRASV12 in the background of either lentiviral shGFP or shMTH1 (KRASV12/shGFP, KRASV12/shMTH1). Blots were probed with the indicated antibodies.

(C) MTH1 suppression reduces KRAS mRNA and protein levels. qPCR analysis is shown from the indicated samples. The black horizontal line indicates a baseline of 1. Two

independent Western blots (representative blots shown in (B)) were quantitated via densitometry using the ImageJ gel analysis module. Normalized fold-changes in protein expression are shown.

(D) MTH1 enhances soft agar colony formation by KRASV12-transformed BEAS2B cells. Representative images, three weeks post-seeding, are shown from the indicated samples to depict extent of colony formation.

(E) Quantitation of results from the soft agar assay depicted in (D), ***$p<0.005$.

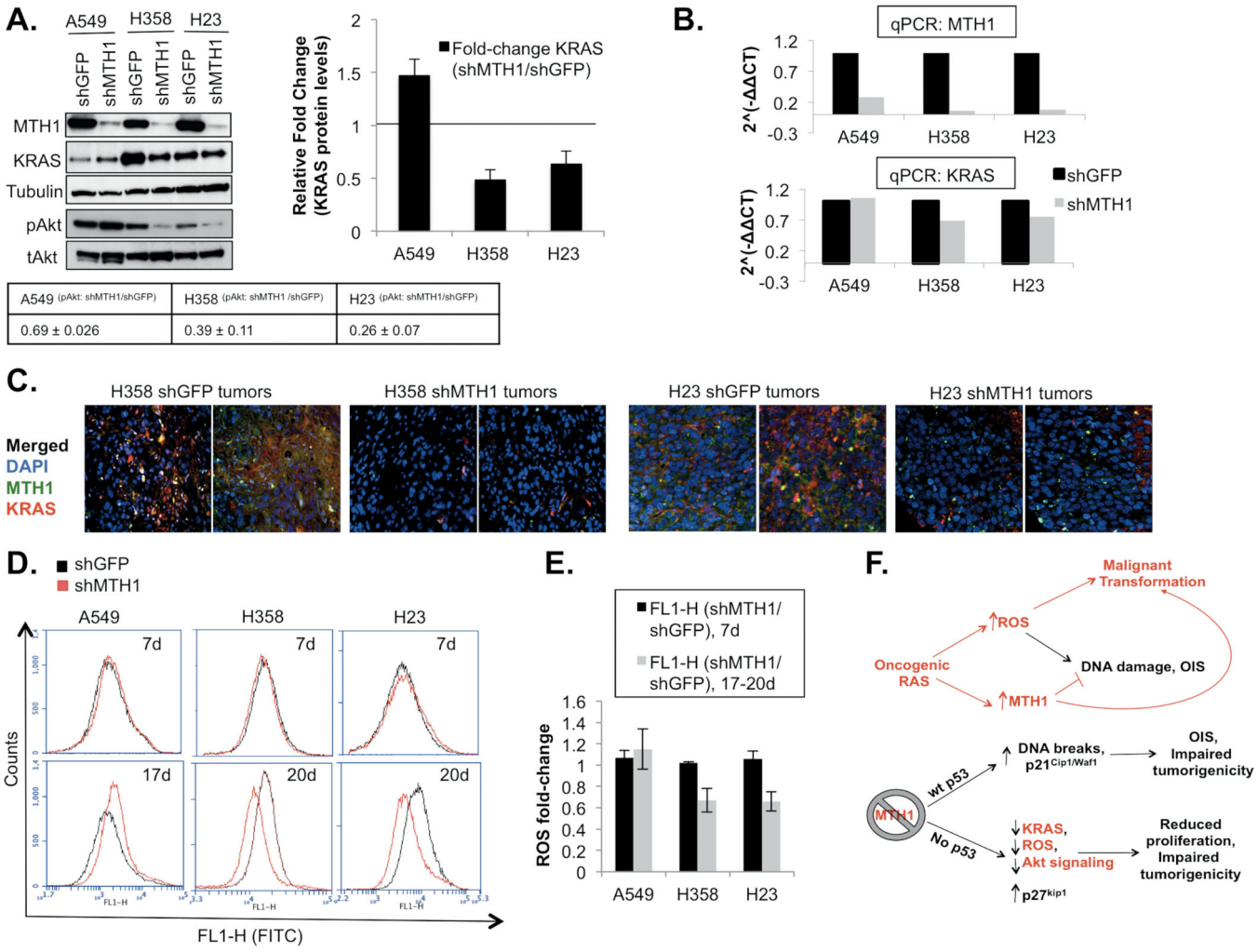

A549 (pAkt: shMTH1/shGFP)	H358 (pAkt: shMTH1 /shGFP)	H23 (pAkt: shMTH1/shGFP)
0.69 ± 0.026	0.39 ± 0.11	0.26 ± 0.07

Figure 5. Proliferation under MTH1 suppression leads to decreased KRAS expression levels *in vitro* and *in vivo*

(A) MTH1 suppression reduces KRAS protein expression in H358 and H23 cells. Approximately 15 μg of protein lysates was immunoblotted against the indicated proteins. Cells from the indicated samples were harvested approximately 18 days following shRNA transduction (11 days for A549 samples). Relative fold-changes in KRAS protein expression in the indicated shMTH1 samples, relative to their counterpart shGFP samples (indicated by the horizontal black line), were calculated by quantitating signal intensities from two independent blots in ImageJ and normalizing to the corresponding GAPDH signal. The table below shows shMTH1-dependent changes in pAkt, normalized to total Akt.

(B) MTH1 suppression reduces KRAS mRNA levels in H358 and H23 cells. Analysis of MTH1 and KRAS mRNA levels was done via qPCR, each sample run in triplicate.

(C) MTH1 suppression reduces *in vivo* KRAS levels. Double immunofluorescent (DIF) staining on H358 and H23 xenograft tumors indicates shMTH1-associated in vivo decrease in KRAS expression. Sections from H23 and H358 xenograft tumors from Fig. 1D were co-stained with DAPI, KRAS (red) and MTH1 (green). A total of 5 sections were stained from

each sample, with two representative sections from each sample being shown at 200X magnification.

(D) Proliferation under MTH1 suppression leads to reduced oncogenic ROS levels. ROS measurements were carried out following CM-DCFDA staining on the indicated samples. Representative profiles and quantitation of relative ROS levels changes are shown from three independent experiments.

(E) Quantitation of relative ROS levels in shMTH1 cells vs. their counterpart shGFP cells, denoted as 'FL1-H (shMTH1/shGFP)', was carried out using the mean FL1 (FITC channel) intensities measured via the BD Accuri software.

(F) Summary of MTH1-mediated molecular effects on oncogenic KRAS-associated pathways. Results are schematically summarized in the context of known oncogenic RAS pathways. Tumor-promoting elements are shown in red and tumor-suppressive elements in black.